Low-temperature crystallization of amorphous $Fe_{68}Cr_{18}Mo_2B_{12}$ alloys

Muhammad Anis
Department of Metallurgy, Engineering Faculty of University of Indonesia

Abstract

A range of microstructure as a result of low-temperature crystallization of amorphous alloy based on the composition $Fe_{68}Cr_{18}Mo_2B_{12}$ prepared by chill block melt spinning casting has been investigated using x-ray diffractometer and transmission electron microscope. Low-temperature crystallization of the amorphous alloy produced a very fine microstructure consisting of α-Fe; body centered tetragonal Fe_3B and a small proportion of orthorhombic Fe_3B. The body centered tetragonal Fe_3B was found to contain fine and coarse faults with lead to streaking in selected area diffraction patterns. The crystallization of the present material is proposed to occur by primary crystallization of solid solution ferritic phase followed by a eutectic reaction of α–Fe + Fe_3B.

Introduction

There is growing interest in the development of metallic glasses (amorphous metals) because of their unique physical and mechanical properties. The work in this area has been reviewed by Ray [1] who developed a new family of alloys based on iron and containing relatively high concentrations of refractory metals and relatively low metalloid concentrations. Such alloys are produced by using high cooling rates during solidification and exhibit extremely high hardness and strength [2].

The as-quenched metallic glasses, which have been rapidly solidified at rates as high as 10^4 to 10^{10} K/s, have a highly disordered structure, which is metastable with respect to the equilibrium crystalline phase. Therefore, these materials are susceptible to structural changes, ie. they transform into a more stable crystalline state. During crystallization which is accompanied by a small increase in density, a decrease in enthalpy and significant changes in most physical properties occur [3]. Most of the useful properties of metallic glass materials usually deteriorate drastically when the amorphous state transforms in a more stable crystalline state [4].

The crystallization mechanisms in metallic glasses have been extensively studied [3,4]. Crystallization occurs by nucleation and growth processes which are governed by diffusion and the types of reactions commonly observed are well illustrated by the hypothetical free energy diagram, as a function of composition, shown in Fig.1 [5], for the Fe-B system. The equilibrium tangent is shown by a solid line and possible metastable equilibria are marked by dashed tangents. Depending of the alloy composition, three possible crystallization reactions can occur and are summarized below:

1. Polymorphous crystallization results in the formation of a supersaturated crystalline alloy or a metastable or stable crystalline compound of the same composition (reaction 1 and 4 in Fig.1). This reaction can occur only in concentration ranges near the pure elements or compounds. The supersaturated phase here will decompose by subsequent precipitation reactions whereas a metastable crystalline compound will undergo phase transformation into the stable equilibrium phases.
2. Primary crystallization of supersaturated solid solution, eg.α-Fe (reaction 2 in Fig.1). During this reaction, the remaining amorphous phase, which is enriched in boron, transform by one of the mechanisms described here.
3. Eutectic crystallization, ie. simultaneous crystallization of two crystalline phases (reaction 3 or 5 in Fig.1) by a discontinuous reaction.

Examples of these three possible crystallization reactions are shown in Fig.2 [5] for three Fe-B metallic glasses.

In the present work, low-temperature crystallization (550 to 700 °C) have been employed for an initially amorphous alloy of composition $Fe_{68}Cr_{18}Mo_2B_{12}$ (at%). This provides the opportunity to examine the more stable phases produced during crystallization at low temperature.

Experimental procedure.

Fragment of ingots, of mass approximately 3-5 g were placed in the bottom of an 18 mm diameter quartz tube drawn down to a fine nozzle and rapidly solidified to thin ribbons by the chill block melt spinning technique. The alloy was melted quickly using a radio frequency induction melting unit, and then the molten alloy was ejected using argon pressure through a small orifice at the bottom of the crucible onto the circumferential surface of the rapidly rotating roll. The orifice was arranged 2-3 mm from the rotating wheel and generally inclined back by up to 15° from the roll radius. Variables employed were chosen to ensure that the ribbon produced was amorphous across the ribbon section. Confirmation that each cast was fully amorphous was obtained by X-ray diffraction (XRD) and by transmission electron microscope (TEM).

Heat treatment were carried out at 550 to 700 °C to devitrify (crystallize) the alloy. For this, samples of ribbon were sealed in quartz tube which have been evacuated and then back-filled with argon to ensure that oxidation was minimized.

The ribbon microstructures were characterized by x-ray diffraction (Philips PW1710 diffractometer) and transmission electron microscope (TEM Jeol 200CX and Philips 400T).

Results.

X-ray diffraction was used to identify the phases present both in the as-cast and heat-treated FeCrMoB ribbons. Fig.3 shows important section of the XRD traces for three different structure of melt spun ribbon, ie. amorphous, a mixture of amorphous and microcrystalline, and microcrystalline, in the as-cast condition. The XRD data for the initially amorphous ribbon after annealing at different temperature are given in Tables 1 to 3. Low-temperature crystallization of the amorphous ribbon, eg. at 550 °C for 0.5 hour, produced metastable orthorhombic Fe_3B, metastable tetragonal Fe_3B and ferrite (see Table 1). The differentiation between the orthorhombic and tetragonal phases is not easy and will be discussed later in association with microstructure analysis using dark field image technique. However, the d spacings of 2.31 Å and 1.98 Å from Table 1 confirmed the presence of orthorhombic Fe_3B whereas the d spacings of 1.93 Å and 1.69 Å from the same table confirmed the presence of tetragonal Fe_3B. The 2.31 Å and 1.98 Å peaks of orthorhombic Fe_3B remain present at 600 °C (see Table 2) but only the 2.31 Å peak remains at 700 °C as can be seen in Table 3. This suggests that the tetragonal Fe_3B has a greater range of temperature stability than the orthorhombic Fe_3B.

Fig.4 shows the general microstructure observed for the amorphous ribbon having nominal composition of $Fe_{68}Cr_{18}Mo_2B_{12}$, which has been annealed at 550 °C for 0.5 hour. XRD traces of this sample indicated complete crystallization and was indexed as α-Fe, orthorhombic Fe_3B and tetragonal Fe_3B. It was extremely difficult to clearly distinguish all the constituents present in the micrograph. Dark field analysis shown in Fig.5 (a) indicates that the ferrite appeared only as small isolated randomly oriented region within the Fe_3B crystals. Furthermore, Fig.5(c) is the dark field image of ferrite + Fe_3B showing the ferrite distribution and a very large Fe_3B particle. Generally, the Fe_3B particles were larger than those of the ferrite.

SADPs were taken from the darkest particle shown in Fig. 6(a) and were indexed as tetragonal Fe_3B. In the dark field analysis using the spot marked A in the SADP shown in Fig.7 (b), the orthorhombic Fe_3B can be distinguished from tetragonal Fe_3B as shown in Fig.7(c). This dark field image clearly shows that the orthorhombic phase occupied a small volume fraction.

Streaking was observed in the diffraction pattern from the ribbon, which was annealed at 550 °C for 0.5 hour, which was derived from some form of faulting in the microstructure. Two types of faulting could be distinguished., the particle with very fine faults as shown in Fig.8 (a) and the particle with coarse faults as shown in Fig.9 (a). SADPs from both micrographs show streaks as shown in Figs.8 (b) and 9 (b). Spots with streaks from these SADPs were indexed and confirmed as

tetragonal Fe_3B spots. Dark field analysis using the spot with streaks in tha SADP in Fig.8 (b) revealed the faulted structure in the dark field image as shown in Fig.8 (d). Another dark field analysis was also performed using the streaks on the SADP in Fig.9 (b) and revealed faults in the dark field image as shown in Fig.9 (c). These observations suggest that the streaks were only derived from the faulting in the tetragonal Fe_3B with no contribution from other phases. It was apparent that the coarse and fine faults were not observed when oriented with a zone axis parallel to the electron beam and hence it was not possible to define the plane on which streaking occurred. It is possible that the morphology of the faults depended on the orientation in which they were observed, although dark field images shown in Fig.8(c) and (d) demonstrate that the faulted structure varied within a particle. However, the exact type of faulting was not clear.

It was concluded that during crystallization, a metastable solid solution α-Fe is formed initially followed by eutectoid decomposition to form α-Fe + tetragonal Fe_3B with a small quantity of orthorhombic Fe_3B which gradually disappeared as the temperature increased.

Discussion.

The amorphous ribbon transformed to a fine supersaturated ferrite solid solution and metastable Fe_3B at 550 °C. Although the low temperature crystallization has been widely studied in Fe-based metallic glasses [5-9] where the transformation products are ferrite solid solution phase and body centered tetragonal Fe_3B which is isomorphous with Fe_3P structure; the mechanism of nucleation and growth of the crystals remains unclear.

In the present work, the amorphous material crystallizes into a ferrite solid solution phase and distribution of body centered tetragonal Fe_3B and orthorhombic Fe_3B phases (Fig.4). As in Fig.9, it would appear that α-Fe crystals grew at a slower rate than the Fe_3B crystals since the α-Fe appeared to be present as isolated crystals within the larger Fe_3B crystals. Walter et al. [10] reported that the low-temperature crystallization products of amorphous $Fe_{40}Ni_{40}P_{14}B_6$ were body centered tetragonal $(Fe,Ni)_3(PB)$ crystals along with a small amount of face centered cubic Ni-Fe solid solution and a trace of α-Fe. They reported that the crystallization occurs by nucleation of body centered tetragonal Fe_3B and since there is more Fe and Ni present than is required to produce only Fe_3B, there are also small amounts of a Ni-Fe face centered cubic phase and some α-Fe. In another article, Walter et al. [11] reported that the crystallization product of amorphous $Fe_{50}Ni_{30}B_{20}$ and $Fe_{80}B_{20}$ is two phases with the cellular structure of the crystalline material derived from essentially eutectic crystallization of the glass; the cells were composed of Fe_3B and α-Fe. The devitrification of amorphous $Fe_{40}Ni_{40}P_{14}B_6$ alloy was also shown to occur by a eutectic reaction [12,13] in this case to austenite (because of the high Ni concentration) and a body centered tetragonal Fe_3B phase. These crystalline phases were very finely spaced: The metastable $(Fe,Ni)_3(PB)$, which is isomorphous with Fe_3P being continuous; and the austenite phase being in rod form. Koster and Herold [14] also reported that crystallization of an amorphous $Fe_{80}B_{20}$ at 300-400 °C occurred by eutectoid reaction producing ellipsoid shaped spherulites which contain small plate-like α-Fe particles embedded in a metastable tetragonal ~ Fe_4B ($Fe_{23}B_6$).

In the present work, the structure of the Fe_3B in $Fe_{68}Cr_{18}Mo_2B_{12}$ alloy was found to be complex since both tetragonal and orthorhombic Fe_3B structures are present. Walter et al. [11] did not observed orthorhombic Fe_3B in crystallization of $Fe_{50}Ni_{30}B_{20}$ and $Fe_{80}B_{20}$. Primary crystallization of α-Fe has been observed [4] followed by eutectic or nearly polymorphous crystallization of tetragonal Fe_3B in $Fe_{80}B_{20}$ foils after in situ annealing in the hot stage of an electron microscope with some orthorhombic Fe_3B which is assumed to occur in the thin foil due to the easier relaxation of stresses induced by the density differences between the amorphous and crystalline phases. This is probably the case for the amorphous $Fe_{68}Cr_{18}Mo_2B_{12}$ alloy. However, the amount of orthorhombic Fe_3B appears to be small as indicated in Fig.7.

The streaks in the diffraction pattern, eg. Figs. 8 (b) and 9 (b) were found to be a result of a fine substructure of tetragonal Fe_3B crystals. It is possible that both the fine (Fig. 8 (a)) and coarse (Fig.9 (a)) faulting are essentially eutectic of α-Fe + tetragonal Fe_3B. If this is the case, it is not clear whether the

low-temperature crystallization occurs by eutectic reaction or by primary crystallization followed by eutectic reaction. The latter would be strongly favoured given the presence of isolated α-Fe.

Walter and Bartram [15] observed that the body centered tetragonal Fe_3B crystals are essentially featureless in the hypoeutectic alloys, eg. $Fe_{85}B_{15}$, $Fe_{84}B_{16}$ and $Fe_{73}Co_{10}B_{17}$. This lack of structure may be related to the fact that crystals of α-Fe nucleated and grew at a lower temperature followed by the nucleation and growth of the Fe_3B crystals at higher temperature. In addition, they also described in the hypereutectic $Fe_{80}B_{20}$ and $Fe_{50}Ni_{30}B_{20}$ alloys, that α-Fe was found in relatively large patches agglomerated within the Fe_3B crystals. In the present work, it is assumed that the $Fe_{68}Cr_{18}Mo_2B_{12}$ alloy can be regarded as a hypoeutectic alloy since the boron content is far from the eutectic composition in the Fe-B system. If this assumption is right, it would appear that the crystallization of this material occurs by primary crystallization of α-Fe and the remaining amorphous matrix which is rich in boron undergoes eutectic reaction of α-Fe + Fe_3B.

Conclusions.

1. At 550 °C for 0.5 hour, the amorphous alloy crystallizes to a very fine microstructure consisting of α-Fe, body centered tetragonal Fe_3B and a small proportion of orthorhombic Fe_3B.
2. The body centered tetragonal Fe_3B contains fine and coarse faults which lead to streaking in selected area diffraction patterns.
3. The crystallization of the present material is proposed to occur by primary crystallization of solid solution ferritic phase followed by a eutectic reaction of α-Fe + Fe_3B.

References.

[1] Ray, R., *European Patent Application*, 0018096, 1980.

[2] Davies, H.A., *Revue de Chimie Minerale*, t.16, 1979.

[3] Scott, M.G., in *Amorphous Metallic Alloys*, Butterworths, London, 1983.

[4] Koster, U., and Herold, U., in *Topics in Applied Physics*, vol.46, Springer-Verlag Berlin Heidelberg, 1981.

[5] Herold, U., Koster, U., in *Rapidly Quenched Metals 3*, vol.1, The Metals Society, 1978.

[6] Bashev, V.F., Miroshnichenko, I.S., and Sergeev, G.A., *Inorganic Materials*, 17, 1981.

[7] Franke, H., Herold, U., Koster, U., and Rosenberg, M., in *Ref.5*.

[8] Kemeny, T., Vincze, I., Fogarrassy, B., and Arajs, S., in *Ref.5*.

[9] Greer, A.L., and Leake, J.A., in *Ref.5*.

[10] Walter, J.L., Rao, P., Koch, E.F., and Bartram, S.F., *Met.Trans.A*, 8A, 1977.

[11] Walter, J.L., Bartram, S.F., and Russel, R.R., Met.Trans.A, 9A, 1978.

[12] Morris, D.G., *Acta Metallurgica*, 29, 1981.

[13] Watanabe, T., and Scott, M., *Jnl.of Mat.Sci.*, 15, 1980.

[14] Koster, U., and Herold, U., *Scripta Metallurgica*, 12, 1978.

[15] Walter, J.L., and Bartram, S.F., in *Ref.5*.

Table 1. XRD data for $Fe_{68}Cr_{18}Mo_2B_{12}$ ribbon after annealing at 550 °C for ½ hour with the corresponding phases present.

d observed (Angstrom)	I/I_1	α-Fe	Fe_3B orthorhombic*	Fe_3B body centered tetragonal+
				6.10
				4.32
				3.84
3.0564	11			3.05
2.7336	10		2.72	2.73
2.3906	11		2.38	2.39
2.2983	8		2.31	
2.1304	19			2.15
2.0925	40		2.10	2.090
2.0723	19		2.05	
2.0290	100	2.0268		2.024
1.9846	15		1.98	
1.9328	30			1.930
1.8838	28		1.88	1.881
1.7565	7		1.75	1.755
1.6945	9			1.692
1.6881	11		1.68	1.686
1.4339	9	1.4332		1.435
1.3492	4			1.347
1.2454	5			1.243
1.1974	3			1.197
1.1727	14	1.1702		

*Bashev et al., Inorganic Materials,17(1981),p.894, with a=6.726, b=4.3311, c=5.468 Å.

+Walter et al.,Met.Trans.A,vol.9A,June 1978,p.803, with a=9.63, c=4.29 Å.

Table 2. XRD data for $Fe_{68}Cr_{18}Mo_2B_{12}$ ribbon after annealing at 600 °C for ½ hour with the corresponding phases present.

d observed (Angstrom)	I/I_1	α-Fe	Fe_3B orthorhombic*	Fe_3B body centered tetragonal+
				6.10
				4.32
				3.84
3.06	7			3.05
2.7306	6		2.72	2.73
2.3887	7		2.38	2.39
2.2998	7		2.31	
2.1582	4		2.18	2.16
2.1323	15			2.15
2.0920	35		2.10	2.090
2.0838	14		2.05	
2.0300	100	2.0268		2.024
1.9845	12		1.98	
1.9335	24			1.930
1.8839	25		1.88	1.881
1.8492	4		1.86	
1.7551	6		1.75	1.755
1.6941	7			1.692
1.6879	9		1.68	1.686
1.4353	9	1.4332		1.435
1.3488	4			1.347
1.2610	3			1.263
1.2440	3			1.243
1.2204	7			1.220
1.1723	12	1.1702		

*Bashev et al.,Inorganic Materials,17(1981),p.894, with a=6.726, b=4.3311, c=5.468 Å.

+Walter et al.,Met.Trans.A,vol.9A,June 1978,p.803, with a=9.63, c=4.29 Å.

Table 3. XRD data for $Fe_{68}Cr_{18}Mo_2B_{12}$ ribbon after annealing at 700 °C for ½ hour with the corresponding phases present.

d observed (Angstrom)	I/I_1	α-Fe	Fe_3B orthorhombic*	Fe_3B body centered tetragonal+
				6.10
				4.32
				3.84
3.06	3			3.05
2.7306	3		2.72	2.73
2.3887	3		2.38	2.39
2.2998	3		2.31	
2.1595	3		2.18	2.16
2.09	17		2.10	2.090
2.03	100	2.0268		2.024
1.9310	8			1.930
1.8828	10		1.88	1.881
1.7563	3		1.75	1.755
1.6879	4		1.68	1.686
1.4360	9	1.4332		1.435
1.3480	3			1.347
1.23	3			1.232
1.2204	3			1.220
1.20	3			1.197
1.1723	12	1.1702		

*Bashev et al.,Inorganic Materials,17(1981),p.894, with a=6.726, b=4.3311, c=5.468 Å.

+Walter et al.,Met.Trans.A,vol.9A,June 1978,p.803, with a=9.63, c=4.29 Å.

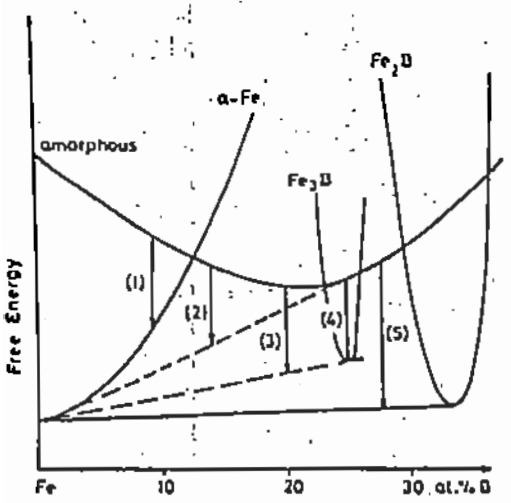

(1) polymorphous crystallization of α-iron
(2) primary crystallization of α-Fe
(3) eutectic crystallization: α-Fe + Fe_3B
(4) polymorphous crystallization of Fe_3B
(5) eutectic crystallization: α-Fe + Fe_2B

Fig.1. Hyppthetical diagram of the free energy for tho various phases in Fe-B alloys versus concentration [5].

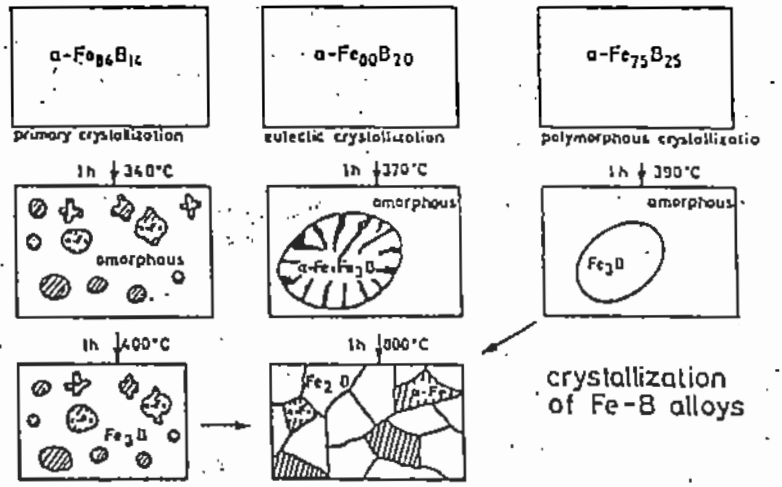

Fig.2. Schematic diagram of typical crystallization reactions in Fe-B alloys [5].

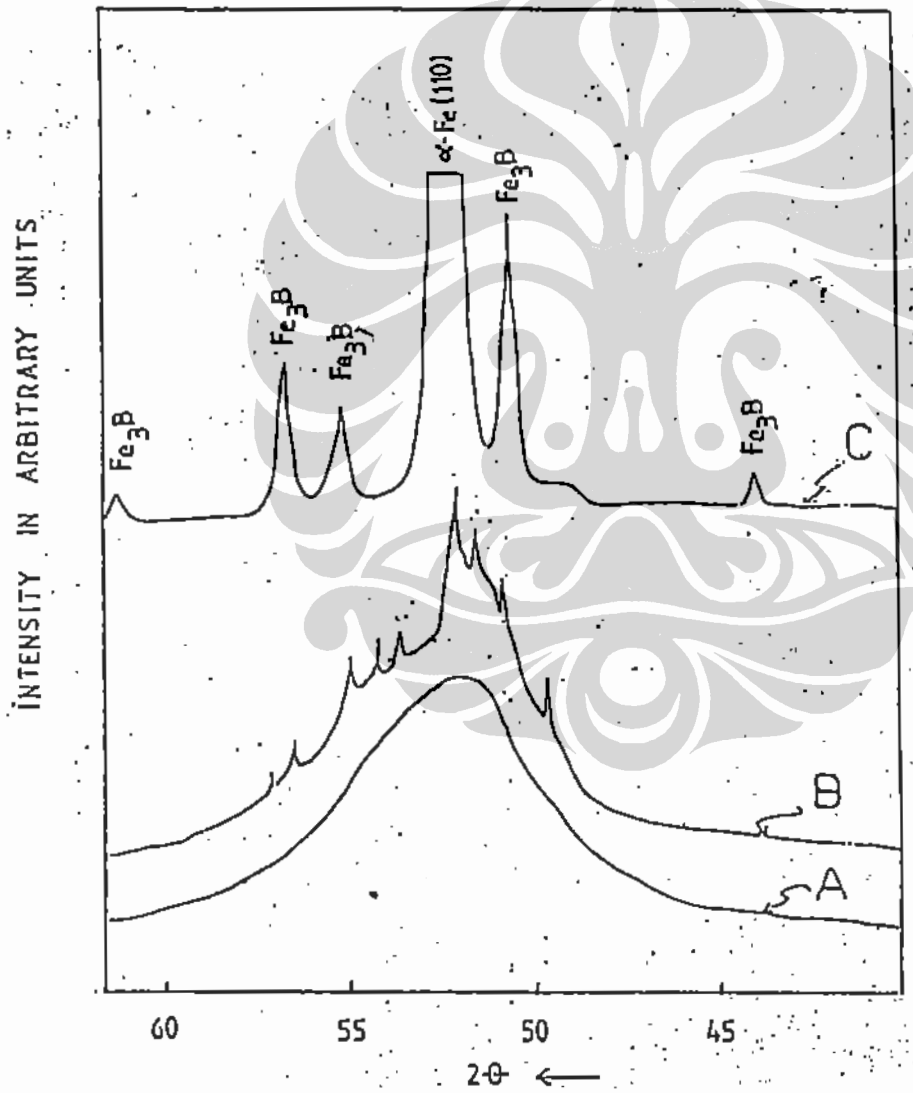

Fig.3. Part of XRD traces for three different melt-spun ribbon thicknesses in the chill surface for $Fe_{68}Cr_{18}Mo_2B_{12}$ in the as-cast condition. (A=15μm;B=15μm;C=15μm)

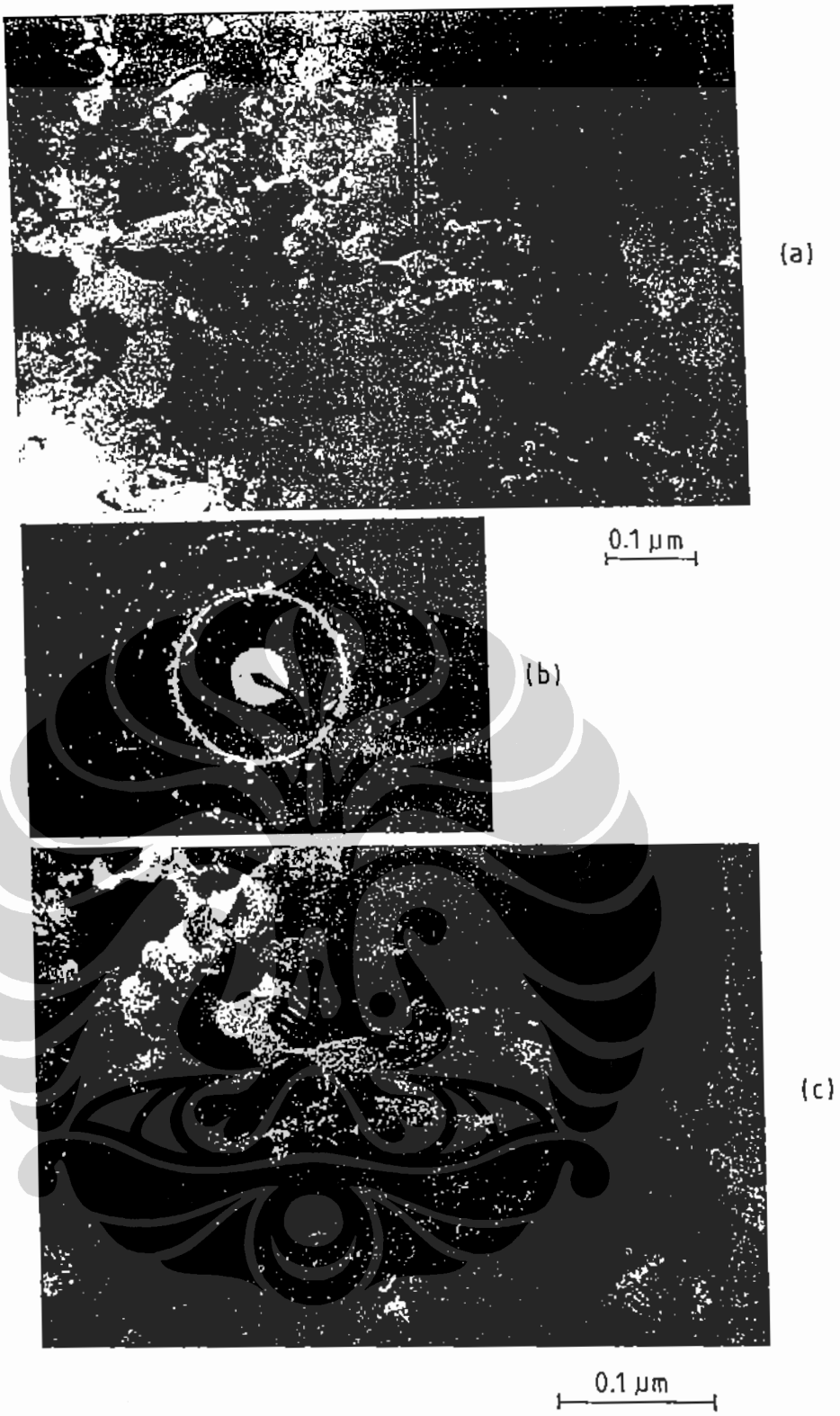

Fig.4. Transmission electron micrograph of the amorphous ribbon which has been annealed at 550 °C for ½ hour.

(a) Bright field image showing the general microstructure
(b) Diffraction pattern of (a)
(c) Bright field image same as (a) at higher magnification.

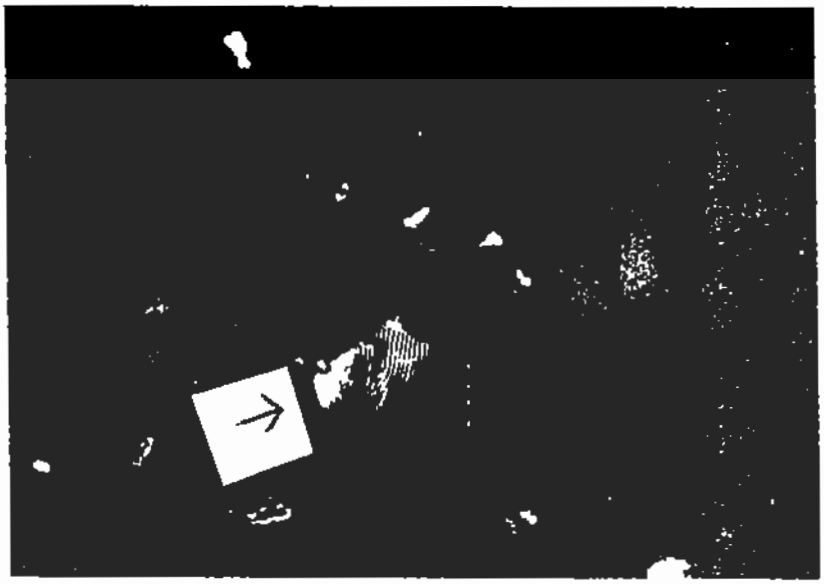

Fig.5. Transmission electron micrograph of the same specimen as in Fig.4.
(a) Dark field image using the first (strongest) ring shown in Fig.4 (b), showing the distribution of ferrite phase
(b) Bright field image of (a)

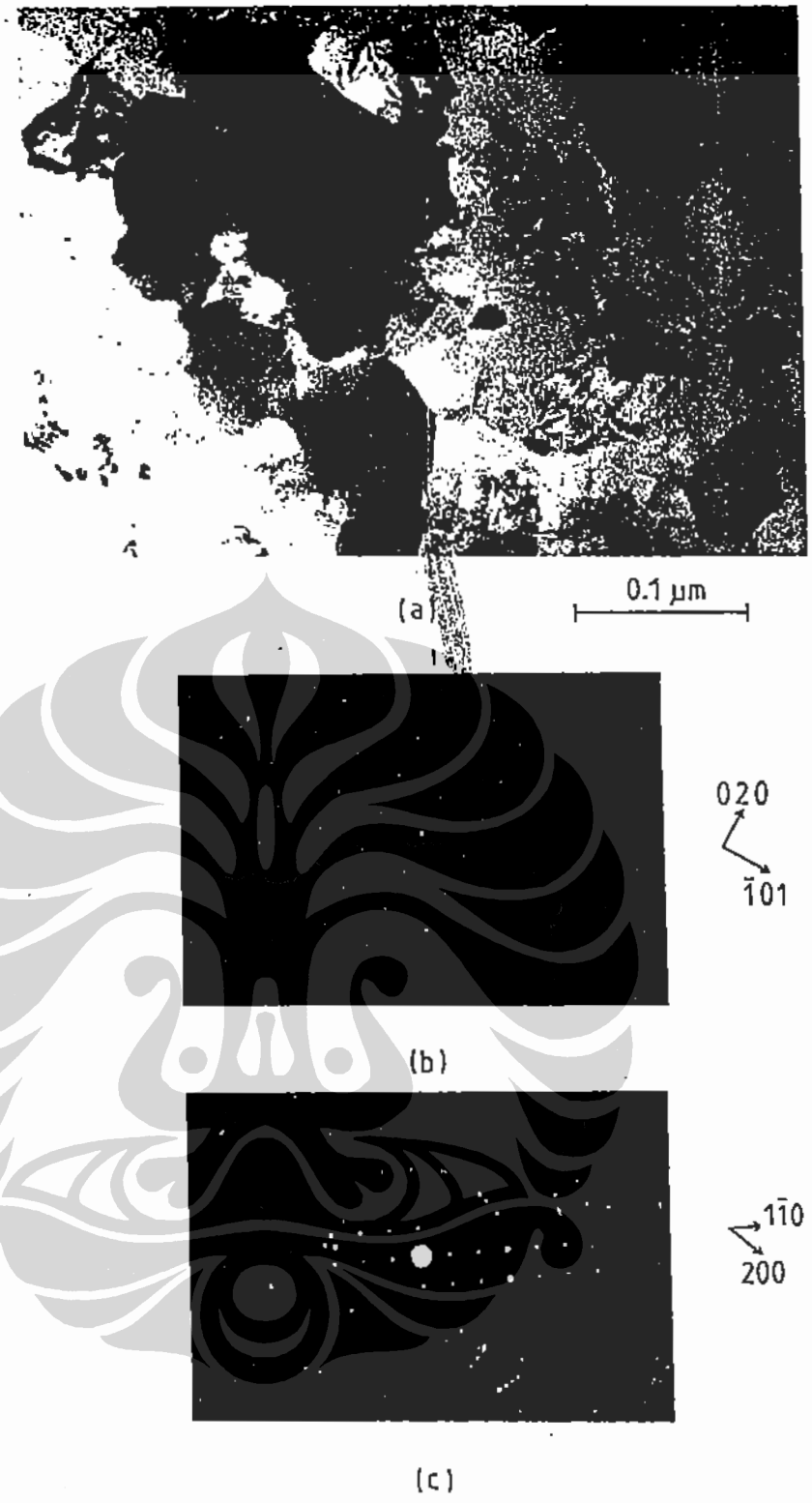

Fig.6. Transmission electron micrograph of the same specimen as in Fig.4.
(a) Bright field image showing the tetragonal Fe_3B
(b) Diffraction pattern of the darkest particle shown in (a) with [101] zone
(c) Another diffraction pattern of [001] zone

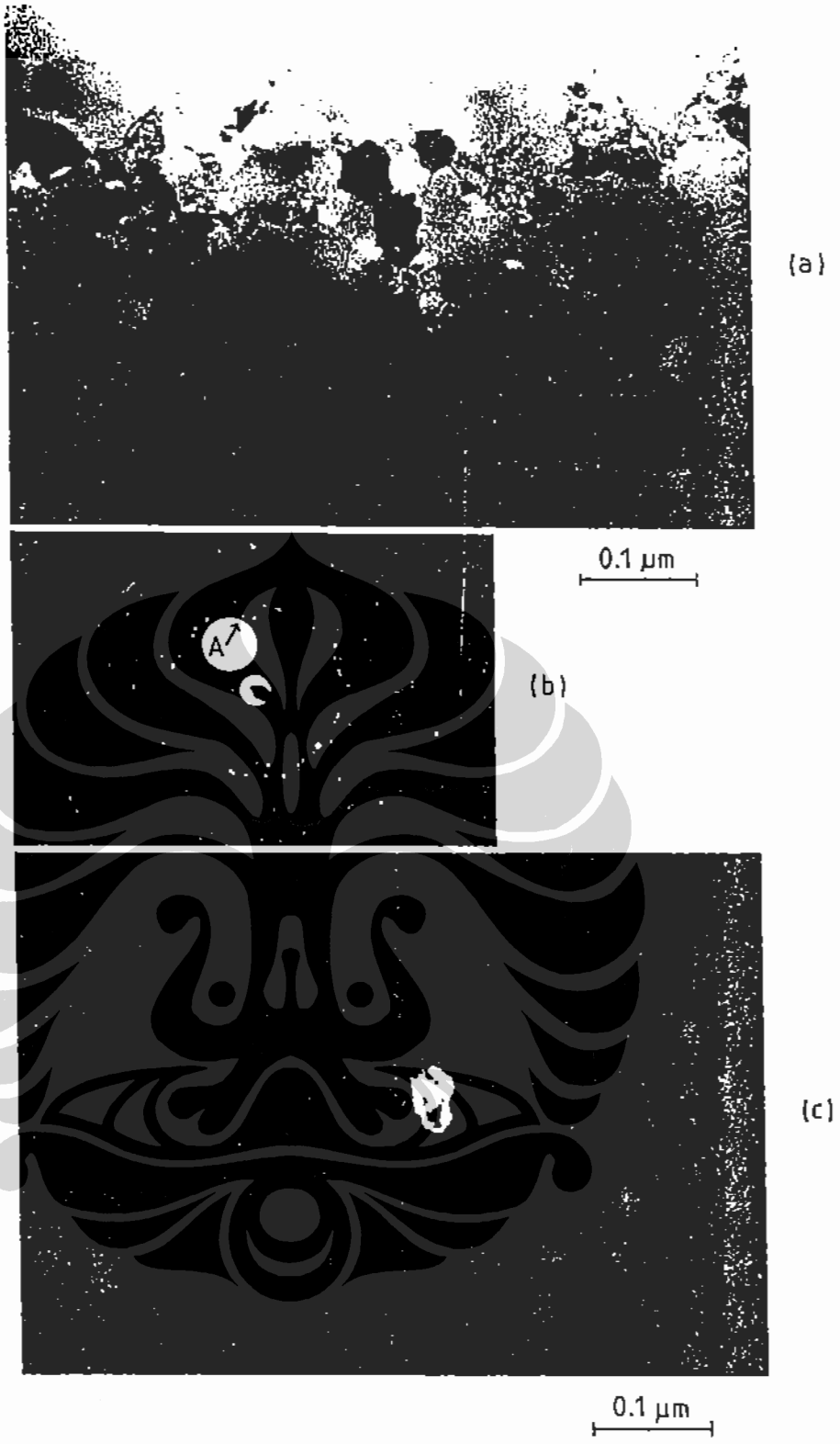

Fig.7. Transmission electron micrograph of the same specimen as in Fig.4.
(a) Bright field image showing orthorhombic Fe_3B indicated by the arrow
(b) Diffraction pattern of (a)
(c) Dark field of (a), using the spot marked A in (b) having d = 1.98 A

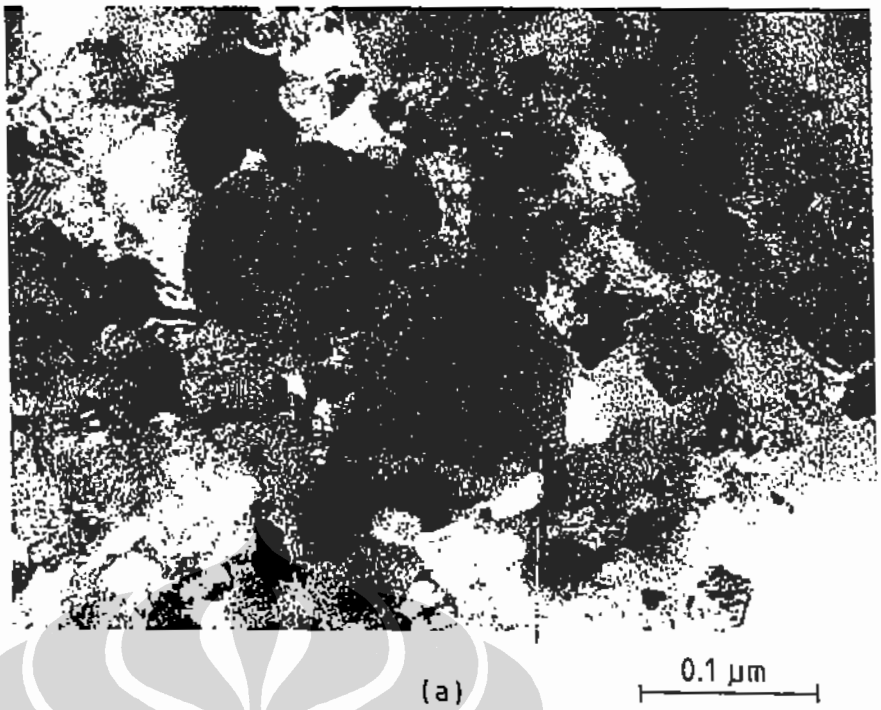

Fig.8. Transmission electron micrograph of the same specimen as in Fig.4.
(a) Bright field image showing particles which contain very fine faults
(b) Diffraction pattern of (a)

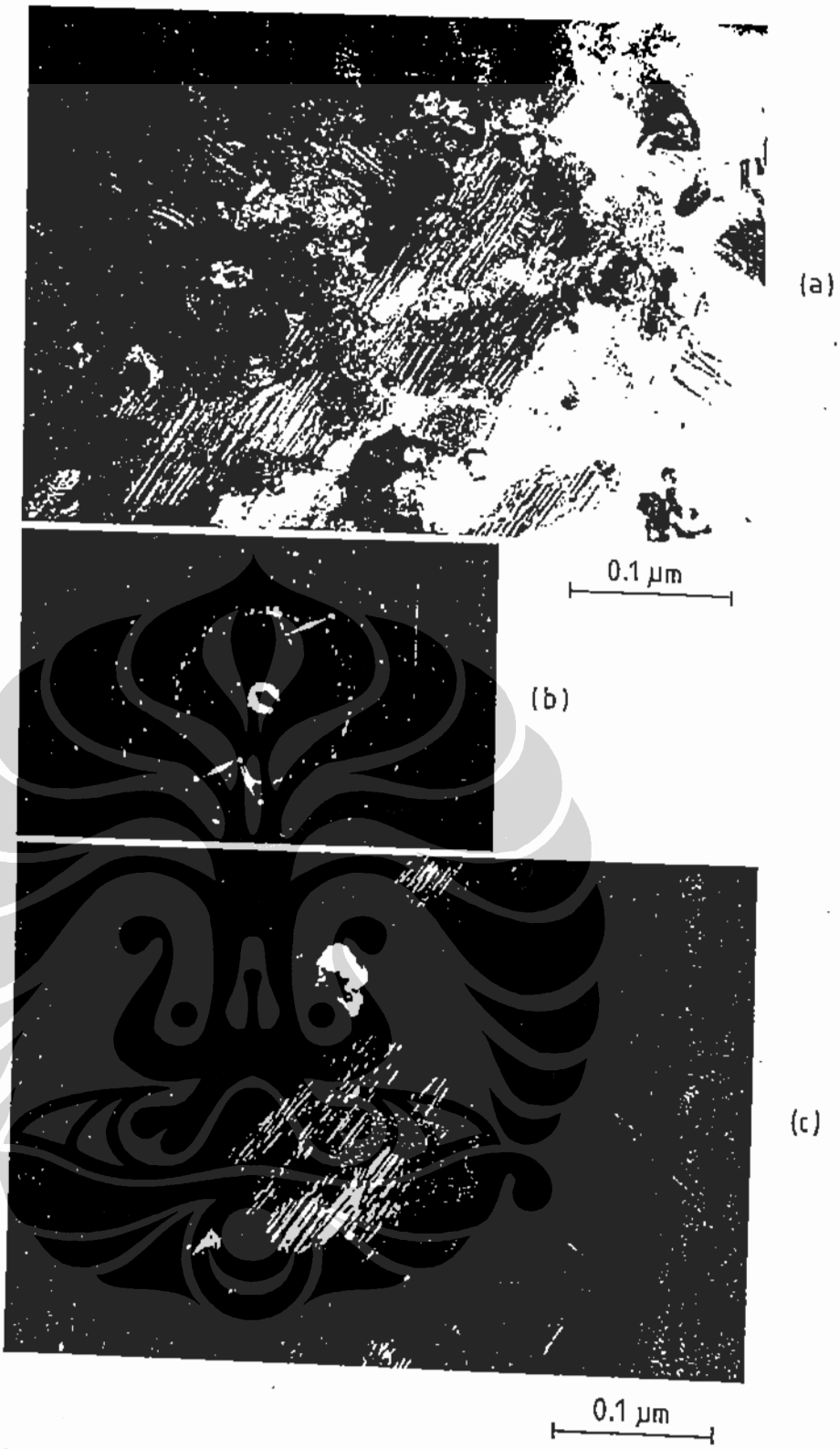

Fig.9. Transmission electron micrograph of the same specimen as in Fig.4.
(a) Bright field image showing particles which contain coarse faults
(b) Diffraction pattern of (a)
(c) Dark field image of (a) using straked spot shown in (b)